

Kinematic Analysis and Optimization of a New Compliant Parallel Micromanipulator

Qingsong Xu & Yangmin Li

Dept. of Electromechanical Engineering, Faculty of Science and Technology, University of Macau, Av. Padre Tomás Pereira S.J., Taipa, Macao SAR, P. R. China
ya47401@umac.mo, ymli@umac.mo

Abstract: In this paper, a new three translational degrees of freedom (DOF) compliant parallel micromanipulator (CPM) is proposed, which has an excellent accuracy of parallel mechanisms with flexure hinges. The system is established by a proper selection of hardware and analyzed via the derived pseudo-rigid-body model. In view of the physical constraints imposed by both the piezoelectric actuators and flexure hinges, the CPM's reachable workspace is determined analytically, where a maximum cylinder defined as an usable workspace can be inscribed. Moreover, the optimal design of the CPM with the consideration of the usable workspace size and global dexterity index simultaneously is carried out by utilizing the approaches of direct search method, genetic algorithm (GA), and particle swarm optimization (PSO), respectively. The simulation results show that the PSO is the best method for the optimization, and the results are valuable in the design of a new micromanipulator.

Keywords: parallel manipulators, compliant mechanism, workspace, kinematic optimization.

1. Introduction

In recent years, global research and development activity on nanotechnology has been growing rapidly due to its potential for revolutionizing the ways in which materials and products are created and the range and nature of functionalities that can be accessed. Different from the macro scale, inertial forces become negligible going down to the nanometer scale, and adhesion forces tend to be larger and dominant. Nanotechnology involves the precise manipulation and control of atoms and molecules to create novel structures with remarkable properties. This influential technology requires a new field termed nanomanipulation to deal with how to handle components and structures in nanometer scale (Fukuda et al., 2003; Sitti, 2001) by utilizing devices with high positioning accuracy and dexterous motion of the end-effector and controlling external forces with sensory feedback, which has been enabled by the invention of scanning tunneling microscopes (STMs), atomic force microscopes (AFMs), and other types of scanning probe microscopes (SPMs).

It is well known that parallel manipulators possess inherent advantages over their serial counterparts in terms of high rigidity, high load carrying capacity, high velocity, and high precision, etc (Merlet, 2000). However, just like any mechanical systems composed of conventional joints, traditional parallel manipulators suffer from errors due to backlash, hysteresis, and manufacturing errors in the joints. Therefore, it is a big challenge to achieve ultra-high precision using conventional joints. Whereas compliant mechanisms, i.e., flexure hinge-based mechanisms, can be employed into

parallel manipulators for ultra precision applications (Kang et al., 2004) thanks to their outstanding characteristics in terms of vacuum compatibility, no backlash property, no nonlinear friction, and ease of manufacture, etc.

Several parallel manipulators employing compliant mechanisms have been designed to perform the manipulation in micro/nanometer scale (Lee and Arjunan, 1991; Tanikawa and Arai, 1999; Yi et al., 2003; Niaritsiry et al., 2004; Li and Xu, 2005a). However, most of the current micromanipulators can provide only a planar 3-DOF motion, or spatial combined motions of translation and rotation. Since the micro- and nano-scale manipulation is usually performed via a microscope, which provides a quite limited field of vision and even a slight rotation of the endeffector will result in the manipulation easily sweeping out of the visual field, the most important motion used in such applications is translational rather than rotary motion. For example, although a dexterous micro-hand is designed by Tanikawa and Arai (1999) to have six DOF, only the translational DOF is utilized in practice. Therefore, a micromanipulator which can provide 3-DOF translational motion with high precision is urgently required for 3-D micro-/nano-scale manipulation.

Our motivation in this work is to develop a new 3-DOF translational compliant parallel micromanipulator (CPM) with an appropriate workspace size and dexterous manipulation for the assembly of micro-/nano-scale components, and to perform the architectural optimization of the CPM with respect to the dexterity and workspace performances.

2. Overview of Optimization Methods

In view of the current optimization problem, it is extremely difficult to express the dexterity performance index into an analytical form, at last there is no analytical expression for the objective function. Thus, it can be regarded as a nonlinear discontinuous optimization problem.

The traditional optimization routine utilizes a local search procedure based on the gradient of the objective function to search for the optimum. For the case of the objective function without a gradient, it can be calculated by a direct search method, such as the famous Nelder-Mead simplex algorithm (Nelder and Mead, 1965). However, the convergence of such techniques heavily depends on good starting guesses, and it faces up the danger of falling into local optima.

On the contrary, the genetic algorithm (GA) can be applied to solve a variety of optimization problems that are not well suited for standard optimization algorithms, including problems in which the objective function is discontinuous, non-differentiable, stochastic, or highly nonlinear, since GA is a global method for solving both constrained and unconstrained optimization problems based on natural evolution (Zhang et al., 2004).

```

Initialize the Population Do {
  For  $i = 1$  to Population Size {
    Calculate fitness value
    If the fitness value is better than the best one
      ( $pBest$ ) in history
    then set current value as the new  $pBest$ 
  }
  Choose the particle with the best fitness value of all the
  particles as  $gBest$ 
  For  $i = 1$  to Population Size {

```

Fig. 1. The pseudocode of a PSO procedure.

Moreover, the particle swarm optimization (PSO) can be employed to solve a variety of optimization problems. As a form of swarm intelligence, PSO is a relatively new algorithm proposed by Kennedy and Eberhart (1995), which is a population-based stochastic optimization technique inspired by the social behavior of bird flocking or fish schooling. Since PSO is originally introduced for the optimization of continuous nonlinear functions, it has been successfully applied to many other problems such as discrete optimization, artificial neural network training, fuzzy system control, and other situations where the evolutionary techniques can be employed (Koay and Srinivasan, 2003). Although PSO owns certain advantages in terms of easy implementation and efficient computation (Eberhart and Shi, 1998; Lovbjerg et al., 2001), the applications of PSO on the issues of manipulator optimal design are still limited. To the

knowledge of the authors, there are no literatures dealing with this area so far.

Since a PSO system is initialized with a population of random solutions and searches for optima by updating generations, it is similar to evolutionary computation techniques such as genetic algorithms (GA). However, compared to GA, PSO has no evolutionary operators such as crossover and mutation. Thus, from the viewpoint of programming, the advantages of PSO are that PSO is easy to implement and there are few parameters to adjust (Birge, 2003).

In the PSO, the population is called a swarm and the individuals (i.e. the search points) are called particles. Each particle moves with an adaptable velocity within the search space, and retains a memory of the best position it ever found. Finally, it knows where the best solution encountered by any other particles in the search space, and will then modify its direction towards its own best position and the global best position, which will provide some forms of convergence to the search. Regarding a D -dimensional search space and a swarm consisting of N particles, the i th particle is represented by a D -dimensional vector $X_i = (x_{i1}, x_{i2}, \dots, x_{iD})$, the velocity of this particle is a D -dimensional vector $V_i = (v_{i1}, v_{i2}, \dots, v_{iD})$, and the best previous position encountered by this particle is described by $P_i = (p_{i1}, p_{i2}, \dots, p_{iD})$. Let g be the index of the particle which attains the best previous position among all the particles in the swarm, and k be the iteration counter. Then, the swarm is manipulated by the equations (Eberhart and Shi, 1998; Clerc and Kennedy, 2002; Hu et al., 2003):

$$V_i(k+1) = wV_i(k) + c_1r_1(P_i(k) - X_i(k)) + c_2r_2(P_g(k) - X_i(k)) \quad (1)$$

$$X_i(k+1) = X_i(k) + V_i(k+1) \quad (2)$$

where w denotes the inertial weight, c_1 and c_2 are the acceleration constants called cognitive and social parameters, respectively, r_1 and r_2 are random numbers uniformly distributed between 0 and 1, and the particle index $i = 1, 2, \dots, N$.

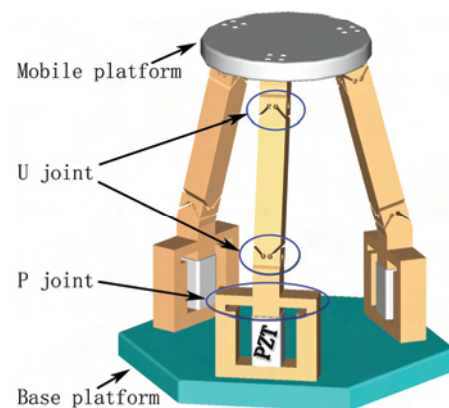


Fig. 2. A 3-PUU CPM.

The selection of the above parameters has been widely studied in the relative literatures (Clerc and Kennedy, 2002; Trelea, 2003), and the pseudocode for a PSO algorithm is elaborated in Fig. 1. In this work, all of these three different approaches will be employed and compared for the optimization of the designed CPM.

3. Description and Development of the CPM

As shown in Fig. 2, the designed 3-DOF CPM using flexure hinges at all joints consists of a mobile platform, a fixed base, and three limbs with identical kinematic structure. Each limb connects the mobile platform to the fixed base by one flexure prismatic (P) hinge and followed by two flexure universal (U) hinges in sequence, where the P joint is fixed at the base and actuated by a piezoelectric (PZT) actuator. Thus, each limb is a PUU kinematic linkage indeed.

It has been shown that a 3-PUU kinematical structure with conventional mechanical joints can be arranged to achieve only translational motions with some certain geometric conditions satisfied (Tsai and Joshi, 2002; Li and Xu, 2005b), i.e., in each kinematic chain, the first revolute (R) joint axis is parallel to the last R joint axis, and the two intermediate R joint axes are parallel to each other. Although the original 3-PUU mechanism is designed using traditional joints for macro-scale applications, it still provides a valuable basis in developing the CPM.

Meeting the geometric conditions, the proposed CPM can provide three translational DOF. Mounting a suitable end-effector on the mobile platform or placing the mobile platform under a specified microscope as a XYZ-stage, the CPM can be used in micro-/nano-scale manipulation. PZT actuators offer the merits involving smooth motion, high accuracy, and fast response, etc., which make them much suitable for precision engineering applications. The drawback of PZT actuators is their limited stroke. To make a compromise between the stroke and resolution and to achieve the goal of this work, one type of PZT, namely, P-239.80, is selected from Polytec PI, Inc., that has the stroke of $140\mu\text{m}$ and resolution of 1.4 nm . The linear actuator of the CPM is implemented with each PZT embedded in a flexure P hinge as shown in Fig. 2.

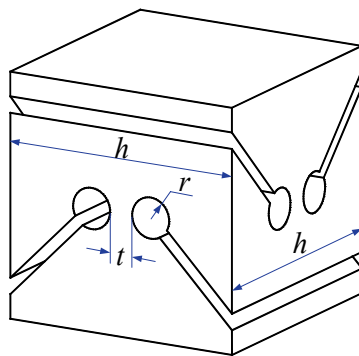


Fig. 3. A flexure U joint.

As illustrated in Fig. 3, the adopted compact flexure U hinge consists of two orthogonally intersected flexure R hinges, and occupies the properties of absence of offset distance between the two R joints and the protection of R joints from over bent. The flexure R hinge can be designed to have profile shapes of right angle, corner filleted, or right circular, etc. Here the right circular one is adopted because its displacement accuracy is the best, i.e., the center of flexure is displaced much smaller than the other types (Lobontiu et al., 2001).

Since the ratio of yield strength (σ_y) to Young's modulus (E) of the material heavily affects the rotary limits of flexure hinge, which will partially determine the manipulator workspace, it is necessary to choose materials with higher ratio of σ_y/E so as to obtain a larger workspace. The material of titanium alloy Ti-6Al-4V is selected to build the CPM.

4. Kinematic Modeling

Pseudo-rigid-body (PRB) model is an effective approach for kinematic design of CPMs, since it allows compliant mechanisms to be modeled as equivalent rigid-link mechanisms and enables the use of traditional mechanism analysis approaches to design compliant mechanisms (Howell, 2001).

4.1 Pseudo-Rigid-Body (PRB) Model

With the mechanism topology identified and each flexure R hinge replaced by a R joint and a torsional spring, the PRB model of the CPM is developed as shown in Fig. 4.

For the sake of analysis, we assign a fixed Cartesian coordinate system $O\{x, y, z\}$ at the centered point O of the fixed base platform $\Delta A_1 A_2 A_3$ with a circumcircle of radius a , and a moving Cartesian frame $P\{u, v, w\}$ on the moving platform at the centered point P of triangle $\Delta B_1 B_2 B_3$ with a circumcircle of radius b . In addition, let the x - and u -axis be parallel to one another, and the x -axis directs along $\overline{OA_1}$. The angle between vectors $\overline{OA_1}$ and $\overline{PB_1}$ is defined as the twist angle θ , i.e., the angle between the mobile platform and the fixed base. The P joints are restricted to move along a direction perpendicular to the base platform so as to obtain a compact architecture. Moreover, in order to generate a symmetric workspace of the manipulator, the twist angle is designed as $\theta = 0^\circ$, the three links $C_i B_i$ are designed to possess equal length of l , and both the base and mobile platforms are assigned to be equilateral triangles.

Within the i th limb, due to the torsion deformation of the spring

with stiffness K_{jk}^i , links j and k act on each other by the torsion moment of M_{jk}^i , that is caused by the angular displacement δ_{jk}^i of the links and can be derived by

$$M_{jk}^i = M_{kj}^i = K_{jk}^i \delta_{jk}^i = K_{jk}^i (\theta_{jk}^i - \theta_{jk}^{i0}) \quad (3)$$

where the stiffness K_{jk}^i can be calculated via the formulation (Paros and Weisbord, 1965):

$$K = \frac{2Eht^{2.5}}{9\pi r^{0.5}} \quad (4)$$

where E denotes the Young's modulus of the material, and parameters h , t and r of flexure hinges are depicted in Fig. 3.

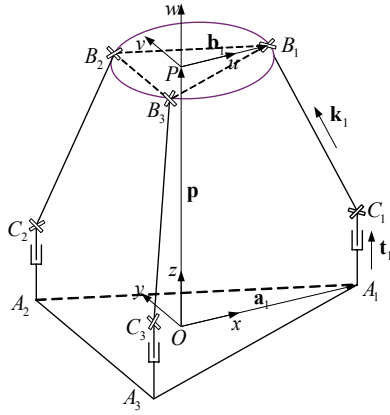


Fig. 4. PRB model of the 3-PUU CPM.

4.2 Kinematic Modeling

Let $\mathbf{q} = [d_1 \ d_2 \ d_3]^T$ be the vector of the three actuated joint variables, and the vector $\mathbf{p} = [x \ y \ z]^T$ of the reference point P be the position of the mobile platform. Given the mobile platform position, the objective of the inverse kinematics problem is to solve the actuated values. Given a set of the actuated inputs, the mobile platform position is solved by the forward kinematics.

Let \mathbf{k}_i denote a unit vector along the leg C_iB_i , d_i represent a linear displacement of the i th actuator, and \mathbf{t}_i denote the corresponding unit vector pointing along A_iC_i . In addition, let $\mathbf{a}_i = \overrightarrow{OA_i}$ and $\mathbf{b}_i = \overrightarrow{PB_i}$. Using a suitable vector-loop analysis, both the inverse and forward kinematics problems have been solved in closed-forms (Li and Xu, 2005b). For example, referring to Fig. 4, a vector-loop equation can be written for the i th limb:

$$l\mathbf{k}_i = \mathbf{s}_i - d_i\mathbf{t}_i \quad (5)$$

where

$$\mathbf{s}_i = \mathbf{p} + \mathbf{b}_i - \mathbf{a}_i \quad (6)$$

Then, in view of (5), the inverse kinematics solutions can be derived as follows:

$$d_i = \mathbf{t}_i^T \mathbf{s}_i - \sqrt{(\mathbf{t}_i^T \mathbf{s}_i)^2 - \mathbf{s}_i^T \mathbf{s}_i + l^2} \quad (7)$$

4.3 Jacobian Matrix Generation

Substituting (6) into (5) and differentiating it with respect to time, yields

$$\dot{d}_i \mathbf{t}_i = \dot{\mathbf{p}} - l \boldsymbol{\omega}_i \times \mathbf{k}_i \quad (8)$$

where $\boldsymbol{\omega}_i$ denotes the vector of angular velocities for link C_iB_i with respect to the fixed frame, and $\dot{\mathbf{p}} = [\dot{x} \ \dot{y} \ \dot{z}]^T$ is the vector of linear velocities for the mobile platform.

Dot-multiplying both sides of (8) by \mathbf{k}_i , leads to

$$\mathbf{k}_i^T \mathbf{t}_i \dot{d}_i = \mathbf{k}_i^T \dot{\mathbf{p}} \quad (9)$$

which can be assembled into a matrix form:

$$\mathbf{B} \dot{\mathbf{q}} = \mathbf{A} \dot{\mathbf{p}} \quad (10)$$

where

$$\mathbf{B} = \begin{bmatrix} \mathbf{k}_1^T \mathbf{t}_1 & 0 & 0 \\ 0 & \mathbf{k}_2^T \mathbf{t}_2 & 0 \\ 0 & 0 & \mathbf{k}_3^T \mathbf{t}_3 \end{bmatrix}, \quad \mathbf{A} = [\mathbf{k}_1^T \ \mathbf{k}_2^T \ \mathbf{k}_3^T]$$

and $\dot{\mathbf{q}} = [\dot{d}_1 \ \dot{d}_2 \ \dot{d}_3]^T$ is the vector of actuated joint rates.

When the manipulator is away from singularities, in view of (10), we can obtain that

$$\dot{\mathbf{q}} = \mathbf{J} \dot{\mathbf{p}} \quad (11)$$

where

$$\mathbf{J} = \mathbf{B}^{-1} \mathbf{A} \quad (12)$$

is the 3×3 Jacobian matrix of a 3-PUU CPM, which relates the output velocities to the actuated joint rates.

5. Workspace Determination

It is well known that parallel manipulators have relatively limited workspace compared with their serial counterparts. Hence it is very important to analyze the shape and volume of the workspace for enhancing applications of parallel manipulators (Ottaviano and Ceccarelli, 2002). The reachable workspace of the 3-PUU CPM is defined as the space that can be reached by the reference point P , and can be determined as follows.

5.1 Workspace Range Subject to Motion Limits of Actuators

Assume the stroke of PZT actuators is Q . Additionally, let the initial positions of PZT actuators be in the case of half stroke, i.e., $-Q/2 \leq d_i \leq Q/2$, for $i = 1, 2$ and 3 .

Combining (5) with (6), we can obtain

$$l\mathbf{k}_i = \mathbf{p} - \mathbf{e}_i \quad (13)$$

where $\mathbf{e}_i = \mathbf{a}_i + d_i\mathbf{t}_i - \mathbf{b}_i$.

Dot-multiplying (13) with itself and rearranging the items, yields

$$\mathbf{p}^T \mathbf{p} - 2\mathbf{p}^T \mathbf{e}_i + \mathbf{e}_i^T \mathbf{e}_i = l^2 \quad (14)$$

which can be expanded into the form:

$$(x-c)^2 + y^2 + (z-d_1)^2 = l^2$$

$$(x+\frac{c}{2})^2 + (y-\frac{\sqrt{3}c}{2})^2 + (z-d_2)^2 = l^2$$

$$(x+\frac{c}{2})^2 + (y+\frac{\sqrt{3}c}{2})^2 + (z-d_3)^2 = l^2 \quad (15)$$

where $c = a - b$.

In view of the range of d_i , each equation in (15) represents the workspace of the corresponding limb, that is a set of spheres with the radii of l . The intersection of three limbs' workspace forms the workspace range of the manipulator restricted by limits of actuators motion range.

5.2 Workspace Range Subject to Rotary Limits of Flexure Hinges

| Flexure hinge parameters (mm) | | |
|--|----------------|--------------------------|
| r | t | h |
| 1.0 | 0.5 | 10.0 |
| P-239.80 piezoelectric actuator parameters | | |
| Stroke Q | Resolution | Push/Pull force capacity |
| 140 μm | 1.4 nm | 4500/500 N |
| Ti-6Al-4V alloy parameters | | |
| Young's modulus | Yield strength | Poisson's ratio |
| 113.8 GPa | 880MPa | 0.342 |

Table 1. Main parameters of flexure hinges, actuators, and Ti alloy.

For the i th PUU kinematic chain at the home position, the two inner revolute joint axes which are parallel to each other are arranged to be perpendicular to the direction of link C_iB_i and lie in plane P_{i1} that is parallel to the z -axis, and the two outer revolute joint axes which are parallel to each other are arranged to be perpendicular to vector $\overline{C_iB_i}$ and lie in plane P_{i2} that is perpendicular to P_{i1} .

Concerning the universal joint C_i , the cone angle of the inner revolute joint is defined as the angle θ_{i1} between link C_iB_i and plane P_{i1} , and cone angle of the outer revolute joint is defined as the angle θ_{i2} between link C_iB_i and plane P_{i2} , respectively. In view of the relationship between normal vectors of the planes and direction vector of the link, the two cone angles can be generated as follows:

$$\theta_{i1} = \sin^{-1} \left(\frac{\mathbf{n}_{i1}^T \mathbf{k}_i}{\|\mathbf{n}_{i1}\|} \right), \quad \theta_{i2} = \sin^{-1} \left(\frac{\mathbf{n}_{i2}^T \mathbf{k}_i}{\|\mathbf{n}_{i2}\|} \right) \quad (16)$$

where \mathbf{n}_{i1} and \mathbf{n}_{i2} denote the normal vectors of plane P_{i1} and P_{i2} , respectively.

Let δ_i^m be the maximum rotary angle of the i th flexure U hinge C_i relative to its initial position angle $\theta_i^0 = \theta_{i1}^0 = \theta_{i2}^0$. The maximum angular displacement arises when the maximum stress σ_{\max} , which occurs at the outermost point of the flexure R hinge section with minimum thickness t , reaches to the yield strength σ_y , i.e.,

$$\sigma_{\max} = \frac{M_i^m(t/2)}{I} = \frac{K_i \delta_i^m(t/2)}{ht^3/12} = \frac{6K_i \delta_i^m}{ht^2} = \sigma_y \quad (17)$$

where $I = ht^3/12$, and the stiffness K_i is calculated by (4). Then, from (17), we can derive that

$$\delta_i^m = \frac{3\pi r^{0.5} \sigma_y}{4Et^{0.5}} \quad (18)$$

which indicates that for a set of parameters of the flexure hinge, the ratio of σ_y/E affects the maximum deflection

δ_i^m greatly.

In view of $|\delta_i| \leq \delta_i^m$, we have

$$-\delta_i^m \leq \theta_{i1} - \theta_{i1}^0 \leq \delta_i^m, \quad -\delta_i^m \leq \theta_{i2} - \theta_{i2}^0 \leq \delta_i^m \quad (19)$$

where $\theta_{i1}^0 = \theta_{i2}^0 = 0$ and $\delta_i^m = \delta^m$ are assumed.

Combining (16) with (19), we can obtain

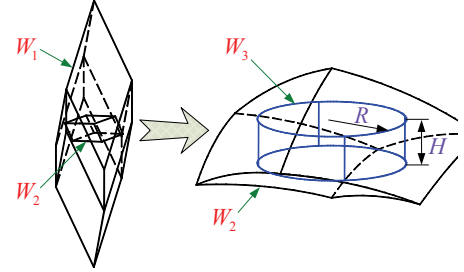


Fig. 5. Representation of workspace determination.

$$\begin{aligned} -ls\delta^m &\leq y \leq ls\delta^m \\ -2ls\delta^m &\leq \sqrt{3}x + y \leq 2ls\delta^m \\ -2ls\delta^m &\leq \sqrt{3}x - y \leq 2ls\delta^m \\ -n_1s\delta^m &\leq (q-d_1)x + c(z-q) \leq n_1s\delta^m \\ -n_2s\delta^m &\leq (q-d_2)(x-\sqrt{3}y)/2 - c(z-q) \leq n_2s\delta^m \\ -n_3s\delta^m &\leq (q-d_3)(x+\sqrt{3}y)/2 - c(z-q) \leq n_3s\delta^m \end{aligned} \quad (20)$$

where s stands for the sine function, $c = a - b$, $q = \sqrt{t^2 - c^2}$, and $n_i = l\sqrt{(q-d_i)^2 + c^2}$, for $i = 1, 2$ and 3 . Equation (20) represents six sets of planes, and the intersection of them forms the workspace range restricted by the rotary limits of flexure universal hinges.

5.3 Determination of Reachable Workspace

The reachable workspace of the 3-PUU CPM can be determined by the intersection of the two ranges expressed by (15) and (20), respectively.

The main parameters of flexure hinges, PZTs, and titanium alloy (Ti-6Al-4V) used to develop the CPM are described in Table 1. In view of the two types of physical constraints discussed above, the workspace determination of the manipulator is illustrated in Fig. 5, where the range W_1 denotes the workspace subjected to rotary limits of flexure hinges, and W_2 represents the workspace range due to motion limits of PZT actuators.

Due to the well elastic nature of the selected material, the range W_1 is larger than W_2 , and the intersection of them forms the manipulator's reachable workspace, i.e., the range of W_2 , which is indeed the range restricted by the constraints of PZT actuators. This is reasonable since the stroke of actuators is fully used. It should be noted that, since the range of W_1 is far larger than W_2 , the material will not be stressed up to the yield point. Otherwise, the allowable stress with a predefined factor of safety has to be considered to determine the workspace of the CPM in

order to ensure that the material will not undergo plastic deformation.

6. Objective Function of the Architectural Optimization

6.1 Usable Workspace Determination

In most situations, the workspace of a manipulator is expressed by a cuboid or a cylinder. Regarding a 3-PUU CPM for micro-/nano-manipulation, the desired workspace is described as a maximum cylinder inscribed within the reachable workspace and defined as the usable workspace, in which most practical applications will be carried out.

The usable workspace of the 3-PUU CPM with a radius of R and height of H is shown in Fig. 5 denoted by W_3 , the volume of which can be calculated by

$$V_u = \pi R^2 \left(Q + \sqrt{l^2 - (R+c)^2} - \sqrt{l^2 - (R-c)^2} \right) \quad (21)$$

where Q is the stroke of PZT actuators, and $c = a - b$.

6.2 Dexterity Measures

The dexterity of a manipulator can be thought as the ability of the manipulator to arbitrarily change its position/orientation, or apply forces/torques in arbitrary directions. And dexterity is an important kinematic performance for the designed CPM in micro- and nano-scale manipulation.

In the literatures, different indices of manipulator dexterity have been introduced. One of the frequently used indices is called kinematic manipulability, which is first proposed for serial manipulators and later extended to parallel robots. Another usually used index is the condition number of the Jacobian matrix, which can be defined as $\kappa = \|\mathbf{J}\| \cdot \|\mathbf{J}^{-1}\|$, with $\|\cdot\|$ denotes the 2-norm of the matrix. As a measure of dexterity, the condition number ranges in value from one (isotropy) to infinity (singularity) and measures the degree of ill-conditioning of the Jacobian matrix, i.e., nearness of the singularity. In addition, the conditioning index (CI) that is defined as the reciprocal of the condition number of the Jacobian matrix, i.e., $\mu = 1/\kappa$, can also be used to evaluate the dexterity of a manipulator. When $\mu = 0$, the manipulator is in a singular configuration, and in the case of $\mu = 1$, the manipulator is in an isotropic configuration. Therefore, the larger the CI, the farther the distance to the singularity, and the more dexterous the manipulator, therefore a global dexterity index (GDI) is given as (Gosselin and Angeles, 1991):

$$GDI = \frac{\int_V \left(\frac{1}{\kappa} \right) dV}{V} \quad (22)$$

where V represents the workspace volume. Since there exist no closed-form solutions for GDI, the integral of the dexterity must be calculated numerically, which can be approximated by a discrete sum:

$$GDI \approx \frac{1}{N_w} \sum_{w \in I'} \frac{1}{\kappa} \quad (23)$$

where w is one of N_w points which are uniformly distributed over the workspace.

6.3 Objective Function

The objective function for optimization is defined as a mixed performance index that is a weighted sum of the usable workspace size (V_u) and the global dexterity index (D_g), i.e.,

$$f(n) = w_u \frac{V_u}{V_{um}} + (1 - w_u) \frac{D_g}{D_{gm}} \quad (24)$$

where the weight parameter w_u ($w_u \in [0, 1]$) describes the proportion of usable workspace size in the mixed index, D_g represents the GDI over the usable workspace, and V_{um} and D_{gm} respectively denote the maximum values of V_u and D_g , which are used to scale the two individual indices into the range of $[0, 1]$.

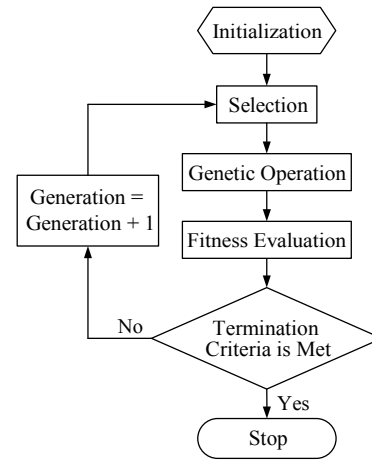


Fig. 6. A flowchart of the GA procedure.

7. Optimization via Different Approaches

The three different approaches in terms of Nelder-Mead simplex method, GA, and PSO have been implemented for the architectural optimization of the 3-PUU CPM based on the objective function $f(n)$ described in (24).

Considering the compactness of the CPM, the base platform size is set to $a = 80$ mm. Three design variables are: the length (l) of each link, the difference ($c = a - b$) between the base and mobile platforms, and the radius (R) of the cylinder usable workspace. Thus, the optimization is a three-dimensional search problem. To ensure a real CPM, the design variables are limited in the search space of: $0 \leq l \leq 200$ mm, $0 \leq c \leq 80$ mm, and 0.03 mm $\leq R \leq 3$ mm, respectively.

7.1 Optimization Settings

Concerning the Nelder-Mead simplex (NMS) method, the starting guess vector $n_0 = [l_0 \ c_0 \ R_0]^T$ for the three variables can be selected from the search space at

random. The termination tolerances for n and $f(n)$ are $1.0\text{E}-6$.

Regarding to the GA approach, normalized geometric selection is adopted, and the genetic operators are chosen to be non-uniform mutation with the ratio of 0.08 and arithmetic crossover with the ratio of 0.8, respectively. In addition, the population size is 50 and the generations' number is set to 300. Fig. 6 shows a flowchart of the GA method.

| | Best fitness | Worst fitness | Mean median | Standard derivation |
|-----|--------------|---------------|-------------|---------------------|
| NMS | 0.499525 | 0.000000 | 0.066611 | 0.172728 |
| GA | 0.499540 | 0.401356 | 0.493429 | 0.020292 |
| PSO | 0.499556 | 0.498273 | 0.499264 | 0.000286 |

Table 2. Optimization results of 30 independent runs from three different approaches.

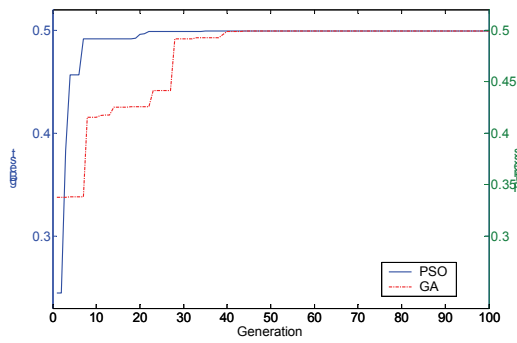


Fig. 7. Convergence of GA and PSO.

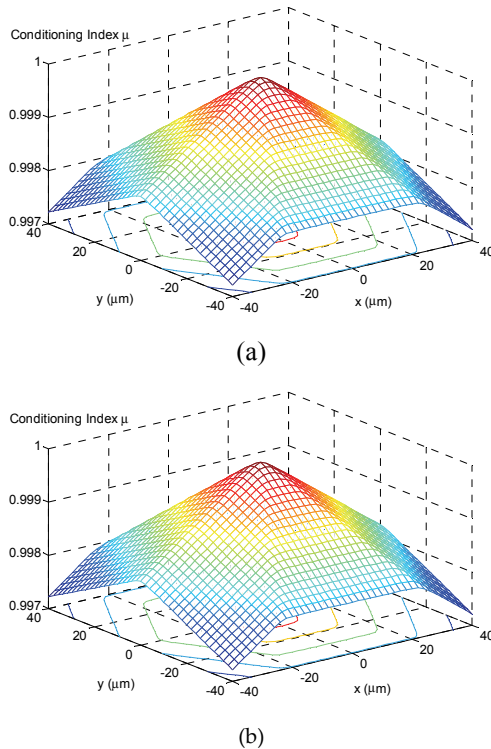


Fig. 8. The conditioning index in typical planes of a (z) = 53.495 mm and (b) z = 53.440 mm.

As far as the PSO method is concerned, the acceleration constants of c_1 and c_2 are set to 2.0, and a linearly decreasing inertial weight starting at 0.7 and ending at 0.4 is used. In order to have a fair comparison between the methods, the generation number is set to 300 and a population size of 50 individuals is also selected for the PSO, since it has been shown that the performances of PSO is not sensitive to the population size (Shi and Eberhart, 1999).

Additionally, both the GA and PSO are initialized with random starting values within the search space.

7.2 Optimization Results

The three optimization processes have been implemented by the developed MATLAB programs, and a total of 30 independent runs have been carried out on a personal computer (Intel Pentium 4 3.0 GHz CPU) for each approach. The inputs to the simulations are the aforementioned parameters and search space, and the outputs are the fitness values with corresponding architectural parameters of the CPM.

Due to the stochastic properties of the Nelder-Mead simplex, GA, and PSO approaches, i.e., they make random choices, the results obtained from each run are different. The best, worst, mean median, and standard deviation of the fitness values for the 30 optimization results from each method are elaborated in Table 2.

It is seen that although the best fitness values obtained from the three approaches are almost the same, the Nelder-Mead simplex algorithm is quite sensitive to the initial guesses which is reflected by the worst and mean fitness, and standard deviation of the results. On the contrary, both the best and worst fitness are closed to the mean value of the PSO results. In addition, the convergent processes of both GA and PSO are illustrated in Fig. 7. It is observed that the GA reaches a convergence after 45 epochs, while the PSO converges quickly within 23 generations.

From the 30 individual simulation results, it can be observed that, although the initial starting values are random, the PSO method always leads to almost the same fitness value which is better than those obtained by the NMS and GA approaches. It also indicates that the PSO has no sensitivity to the initial conditions like the Nelder-Mead simplex means. And the PSO has a better convergence rate than a GA procedure. Clearly, PSO is the best approach for the architectural optimization of a 3-PUU CPM. The optimized parameters of the CPM are: $l = 92.488$ mm, $c = 75.516$ mm, and $R = 0.030$ mm.

7.3 Dexterity Verification

The distribution of conditioning index (μ) in the top and bottom planes ($z = 53.495$ mm and $z = 53.440$ mm) has a maximum value approximately up to 1 when the mobile platform lies in the z -axis, which decreases as the platform approaches to the workspace boundary. Furthermore, each value of μ in any planes is larger than

0.997 and very close to 1, and the variation is very slight. It indicates that there exist no singular configurations in the usable workspace, within which the manipulator can perform a high dexterous manipulation.

8. Conclusions

A new 3-DOF translational compliant parallel micromanipulator utilizing flexure hinges has been presented in this paper. The system is designed by a proper choice of actuators, flexure hinges and the material, and modeled via the PRB model. Taking into account the physical constraints introduced by the PZT actuators stroke and the material elasticity, the workspace range of the CPM is generated analytically. In order to obtain a large usable workspace that is defined as the maximum inscribed cylinder within the reachable workspace with a large global dexterity index, the architecture parameters of the CPM have been optimized using three different approaches of Nelder-Mead simplex, GA, and PSO, respectively. The simulation results show that the PSO is an efficient method for the architectural optimization of the CPM, since PSO can obtain the best fitness value of the objective function with a better convergence rate and has no sensitivity to the initial guesses, which results in a manipulator performing a high dexterous manipulation within the usable workspace. This is also the reason why the PSO is adopted for the optimization problem of the parallel manipulator.

The main contribution of this paper lies in the novel design and kinematic analysis of a 3-PUU CPM, and the architectural optimization through a new approach, i.e., the particle swarm optimization. In the future work, the CPM will be investigated in more detail in terms of statics and stiffness analyses, and the PRB model will be compared with the finite element model of the CPM to arrive at the actual deformations of the links due to the actuation forces.

Acknowledgment: The authors appreciate the fund support from the research committee of University of Macau under grant no.: RG068/05-06S/LYM/FST and Macao Science and Technology Development Fund under grant no.: 069/2005/A.

9. References

- Birge, B. (2003). PSOT – a particle swarm optimization toolbox for use with Matlab, in Proc. of IEEE Swarm Intelligence Symposium, pp. 182–186.
- Clerc, M. & Kennedy, J. (2002). The particle swarm-explosion, stability, and convergence in a multidimensional complex space, *IEEE Trans. Evol. Comput.*, Vol. 6, No. 1, pp. 58–73.
- Eberhart, R. C. & Shi, Y. (1998). Comparison between genetic algorithms and particle swarm optimization, in Proc. of 7th Int. Conf. on Evolutionary Programming VII, pp. 611–616.
- Fukuda, T., Arai, F. & Dong, L. (2003). Assembly of nanodevices with carbon nanotubes through nanorobotic manipulations, *Proc. of the IEEE*, Vol. 91, No. 11, pp. 1803–1818.
- Gosselin, C. & Angeles, J. (1991). A global performance index for the kinematic optimization of robotic manipulators, *ASME J. Mech. Des.*, Vol. 113, No. 3, pp. 220–226.
- Howell, L. L. (2001). *Compliant Mechanisms*, Wiley, New York.
- Hu, X., Eberhart, R. C. & Shi, Y. (2003). Engineering optimization with particle swarm, in Proc. of IEEE Swarm Intelligence Symposium, pp. 53–57.
- Kang, B. H., Wen, J. T., Dagalakakis, N. G. & Gorman, J. J. (2004). Analysis and design of parallel mechanisms with flexure joints, in Proc. of IEEE Int. Conf. on Robotics and Automation, pp. 4097–4102.
- Kennedy, J. & Eberhart, R. C. (1995). Particle swarm optimization, in Proc. of Int. Conf. on Neural Networks, pp. 1942–1948.
- Koay, C. A. & Srinivasan, D. (2003). Particle swarm optimization-based approach for generator maintenance scheduling, in Proc. of IEEE Swarm Intelligence Symposium, pp. 167–173.
- Lee, K. M. & Arjunan, S. (1991). A three-degrees-of-freedom micromotion in-parallel actuated manipulator, *IEEE Trans. Robot. Automat.*, Vol. 7, No. 5, pp. 634–641.
- Li, Y. & Xu, Q. (2005a). Design and analysis of a new 3-DOF compliant parallel positioning platform for nanomanipulation, in Proc. of 5th IEEE Conf. on Nanotechnology, pp. 126–129.
- Li, Y. & Xu, Q. (2005b). Kinematic analysis and dynamic control of a 3-PUU parallel manipulator for cardiopulmonary resuscitation, in Proc. of 12th Int. Conf. on Advanced Robotics, pp. 344–351.
- Lobontiu, N., Paine, J. S. N., Garcia, E. & Goldfarb, M. (2001). Corner-fillet flexure hinges, *ASME J. Mech. Des.*, Vol. 123, No. 3, pp. 346–352.
- Lovbjerg, M., Rasmussen, T. K. & Krink, T. (2001). Hybrid particle swarm optimiser with breeding and subpopulations, in Proc. of 3rd Genetic and Evolutionary Computation Conf., pp. 469–476.
- Merlet, J.-P. (2000). *Parallel Robots*, Kluwer Academic Publishers, London.
- Nelder, J. A. & Mead, R. (1965). A simplex method for function minimization, *Computer Journal*, Vol. 7, pp. 308–313.
- Niaritsiry, T.-F., Fazenda, N. & Clavel, R. (2004). Study of the sources of inaccuracy of a 3DOF flexure hinge-based parallel manipulator, in Proc. of IEEE Int. Conf. on Robotics and Automation, pp. 4091–4096.
- Ottaviano, E. & Ceccarelli, M. (2002). Optimal design of CaPaMan (Cassino Parallel Manipulator) with a specified orientation workspace, *Robotica*, Vol. 20, No. 2, pp. 159–166.
- Paros, J. M. & Weisbord, L. (1965). How to design flexure hinges, *Machine Design*, Vol. 37, pp. 151–156.
- Shi, Y. & Eberhart, R. C. (1999). Empirical study of particle swarm optimization, in Proc. of 1999 Congress on Evolutionary Computation, pp. 1945–1950.
- Sitti, M. (2001). Survey of nanomanipulation systems, in Proc. of 1st IEEE Conf. on Nanotechnology, pp. 75–80.
- Tanikawa, T. & Arai, T. (1999). Development of a micro-manipulation system having a two-fingered micro-hand, *IEEE Trans. Robot. Automat.*, Vol. 15, No. 1, pp. 152–162.
- Trelea, I. C. (2003). The particle swarm optimization algorithm: Convergence analysis and parameter selection, *Information Processing Letters*, Vol. 85, No. 6, pp. 317–325.
- Tsai, L. W. & Joshi, S. (2002). Kinematics analysis of 3-DOF position mechanisms for use in hybrid kinematic machines, *ASME J. Mech. Des.*, Vol. 124, No. 2, pp. 245–253.
- Yi, B.-J., Chung, G. B., Na, H. Y., Kim, W. K. & Suh, I. H. (2003). Design and experiment of a 3-DOF parallel micromechanism utilizing flexure hinges, *IEEE Trans. Robot. Automat.*, Vol. 19, No. 4, pp. 604–612.
- Zhang, D., Xu, Z., Mechefske, C. M. & Xi, F. (2004). Optimum design of parallel kinematic toolheads with genetic algorithms, *Robotica*, Vol. 22, No. 1, pp. 77–84.